

Flipping electric dipole in the vibrational wave packet dynamics of carbon monoxide

Carlos Barbero-Petrel,¹ Peter Schmelcher,^{2,3} and Rosario González-Férez^{1,4}

¹*Departamento de Física Atómica, Molecular y Nuclear, Universidad de Granada, 18071 Granada, Spain*

²*Zentrum für Optische Quantentechnologien, Universität Hamburg, Luruper Chaussee 149, 22761 Hamburg, Germany*

³*The Hamburg Centre for Ultrafast Imaging, Universität Hamburg, Luruper Chaussee 149, 22761 Hamburg, Germany*

⁴*Instituto Carlos I de Física Teórica y Computacional, Universidad de Granada, 18071 Granada, Spain*

(Dated: March 8, 2024)

Recently Rydberg atom-ion bound states have been observed using a high resolution ion microscope (Nature **605**, 453 (2022)) and the corresponding vibrational dynamics has been spectroscopically analyzed. The atom-ion bond is created by an avoided crossing, which involves a flipping molecular dipole. Motivated by the discovery of this binding mechanism we address here the question whether a similar behavior can also occur for ground state diatomic molecules. Specifically, we investigate the vibrational wave packet dynamics within the $^1\Sigma_g^+$ electronic ground-state of carbon monoxide (CO), which shows a zero crossing of its dipole moment function close to its equilibrium. Via time-evolution of coherent states we demonstrate that indeed a flipping dipole is obtained and its dynamics can be controlled to some extent. Varying the coherent state parameter we explore different regions of the vibrational excitation spectrum thereby tuning the time scales of the rapid oscillatory motion of the relevant observables, their decay and revivals as well as the transition to a regime of irregular dynamics.

I. INTRODUCTION

As a consequence of the many decade-long investigations on the theory of the electronic structure of molecules [1, 2] we have now a profound understanding of the molecular binding mechanisms including the paradigms of covalent, ionic and correlation-based binding. While these achievements have enabled us to steadily advance to increasingly larger molecular systems thereby covering more and more of the chemically relevant landscape of molecules by using in particular coupled cluster [3] and density functional theory [4] a parallel development has taken place, which opens up the route of exploring synthetic quantum systems. One major category of synthetic quantum systems are those based on neutral ultracold quantum matter [5]. Cooling, trapping and controlling the interactions among atoms [6, 7] allows not only to prepare designated many-body quantum systems [8], which is at the heart of quantum simulation [9], but opens also the pathway of preparing novel kinds of few-body atomic and molecular systems. Among these are weakly bound ultracold species, such as Efimov states [10] but in particular also molecular species that have highly-excited Rydberg atoms as a basic ingredient [11]. One outstanding category of species are the so-called ultralong-range Rydberg molecules composed of a Rydberg atom and one to many neutral ground state atoms [12]. These highly asymmetric and hugely extended molecules were first predicted theoretically [13] and subsequently observed experimentally almost a decade later [14]. They can be divided into low angular momentum non-polar and high angular momentum polar Rydberg molecules where the binding is established through the low-energy scattering of the Rydberg electron off the ground state atoms. A plethora of intriguing properties of these ultralong-range molecules have been found in the past decade rendering them a laboratory for

novel binding mechanisms and dynamical processes on extraordinary length and time scales [15–23].

Very recently the binding of an atomic ion to a Rydberg atom has been predicted [24, 25] and experimentally observed [26]. The underlying binding mechanism is different from the above-mentioned ones. The positively charged ion interacts with the Rydberg dipole moment, which varies substantially across the potential well that contains the corresponding vibrational bound states. The Rydberg atoms dipole moment thereby covers a range of negative and positive values due to the fact that an avoided crossing between low- and high-angular momentum states is responsible for the formation of the underlying potential well. This has been resolved in an ion microscope thereby imaging the radial extent and angular alignment of the molecule [26]. In a next step the vibrational and orientational dynamics of the Rydberg atom-ion-molecules has been probed [27] using the high resolution ion microscope.

Motivated by the above-mentioned analysis of the bonding mechanism of the Rydberg atom-ion-molecule the natural question appears whether similar properties could also appear for 'traditional' ground state diatomic molecules. More specifically, could one obtain an oscillating and flipping dipole for a vibrational wave packet oscillating in the corresponding ground state potential energy curve shown in Fig. 1 (a). To answer this question we address in this work the wave packet dynamics taking place in the potential energy curve of the electronic $^1\Sigma_g^+$ ground state of the carbon monoxide molecule (CO). The latter is known to change the character of its bond from covalent around the equilibrium position to ionic for larger internuclear distances. More specifically, we choose CO as a prototype due to its electric dipole moment (EDM) function $D(R)$ shown in Fig. 1 (b). The EDM possesses a zero crossing close to its equilibrium internuclear distance (see Fig. 1 (a)) and becomes substantially negative

and positive for smaller and larger internuclear distances, respectively. It reaches a maximum for an internuclear distance which is almost two times the equilibrium one. As a consequence, it has been shown in a previous work that the impact of an electric field strongly depends on its vibrational excitation: the energetically lowest-lying states become anti-oriented with respect to the field direction, whereas higher excited ones are oriented [28].

In the present work we employ initial wave packets that are coherent states of a harmonic oscillator potential related to the potential energy curve of the electronic ground state of CO and propagate them in time to explore their dynamical properties. Depending on the parameter values of the coherent states they cover different regimes of the vibrational eigenspectrum and possess an oscillating EDM that changes sign in the course of its dynamical evolution. Our analysis covers the complete dynamics including short time oscillations, decay and (fractional) revivals accompanied by a characteristic spreading and refocusing of the wave packet as well as, and in particular, their characteristic dipole dynamics.

The paper is organized as follows. In Sec. II, we describe the Hamiltonian, initial wave packet and the expectation values used to explore the corresponding time evolution. In Sec. III, the vibrational wave packet dynamics is analyzed with varying coherent state parameters thereby addressing regimes of different dynamical behaviour. Our conclusions are presented in Sec. IV.

II. VIBRATIONAL DYNAMICS AND COHERENT STATE

Within the Born-Oppenheimer approximation, the Hamiltonian of the rovibrational motion of a diatomic molecule reads

$$H = -\frac{\hbar^2}{2\mu R^2} \frac{\partial}{\partial R} \left(R^2 \frac{\partial}{\partial R} \right) + \frac{\mathbf{N}^2}{2\mu R^2} + V(R) \quad (1)$$

where the first and second terms represent the vibrational and rotational kinetic energies, \mathbf{N} is the rotational angular momentum, R the internuclear coordinate, and μ the reduced mass. The electronic potential energy curve $V(R)$ of the ground-state of CO is presented in Fig. 1 (a) [29]. Here, we focus on states with no rotational excitations $N = 0$, and analyze the corresponding vibrational wave packet dynamics with an emphasis on the dynamics of the dipole of the wave packet.

In addition to the reduced (w.r.t. the integration measure involving R) Schrödinger equation belonging to the Hamiltonian (1) and the resulting vibrational eigenstates, we employ complementary a one-dimensional harmonic oscillator potential that approximates the electronic ground-state potential of CO around its equilibrium. Our initial wave packet is a coherent state of this fitted harmonic oscillator potential. In position represen-

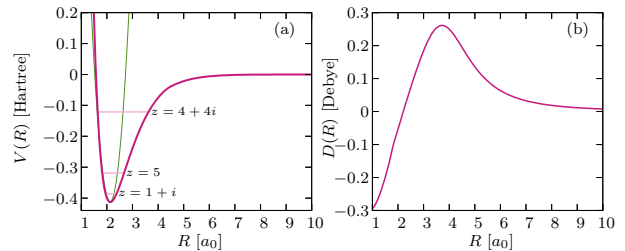


FIG. 1. For carbon monoxide, we show (a) the electronic ground-state potential curve (thick pink line), and the corresponding fitted harmonic oscillator potential (thin green line), and (b) the electric dipole moment function. In panel (a) the horizontal lines indicate the energies of the coherent states together with their parameter values z .

tation this coherent state reads [30, 31]

$$\psi_z(R) = \sqrt{\frac{\alpha}{\sqrt{\pi}}} \exp \left[-\frac{(|z|^2 - z^2)}{2} \right] \times \exp \left[-\frac{(\alpha(R - R_0) - \sqrt{2}z)^2}{2} \right], \quad (2)$$

where $\alpha = \sqrt{\mu\omega/\hbar}$ is the inverse of the harmonic oscillator length, ω the frequency of the fitted harmonic oscillator, and $R_0 = 2.13 a_0$ corresponds to the position of the minimum of the electronic ground state potential energy curve of CO. The coherent state is an eigenstate of the annihilation operator, and z , which can take complex values, is the corresponding eigenvalue. In this work, we explore the wave packet dynamics of this coherent state by varying z and thereby cover different dynamical regimes.

For a given value of z , the coherent state is expanded in the, admittedly incomplete, basis formed by the vibrational eigenfunctions $\varphi_\nu(R)$ of the CO molecule as

$$\psi_z(R) = \sum_{\nu=0}^{\nu_{max}} c_\nu^z \varphi_\nu(R), \quad (3)$$

where ν is the vibrational quantum number and $c_\nu^z = \langle \varphi_\nu(R) | \psi_z(R) \rangle$. The vibrational (reduced) eigenfunctions $\varphi_\nu(R)$ are obtained by solving the time-independent Schrödinger equation belonging to the Hamiltonian in Eq. (1). Note that the electronic ground state of CO possesses more than 80 bound vibrational levels for $N = 0$, and in our calculations we take $\nu_{max} = 82$. However, only the set of vibrational states with $|c_\nu^z| \gtrsim 0.01$ have a significant impact on the dynamics, and this set strongly depends on the chosen value of z . Of course, the coherent state is only approximated by the expansion (3) and, however, we cover the coherent state with an accuracy above 99.99% of the corresponding overlap.

Since the Hamiltonian is time-independent, the time

evolution of the coherent state is given by

$$\Psi_z(R, t) = \sum_{\nu=0}^{\nu_{max}} c_{\nu}^z \varphi_{\nu}(R) e^{-itE_{\nu}/\hbar}, \quad (4)$$

where E_{ν} is the eigenvalue associated to the eigenstate $\varphi_{\nu}(R)$. The vibrational dynamics is analyzed by inspecting the expectation values $\langle R \rangle_t = \langle \Psi_z(R, t) | R | \Psi_z(R, t) \rangle$ and $\langle D(R) \rangle_t = \langle \Psi_z(R, t) | D(R) | \Psi_z(R, t) \rangle$, with $D(R)$ being the EDM of CO [32]. Their temporal evolution is encapsulated in the general equation

$$\begin{aligned} \langle f(R) \rangle_t &= \langle \Psi_z(R, t) | f(R) | \Psi_z(R, t) \rangle = \\ &\sum_{\nu=0}^{\nu_{max}} |c_{\nu}|^2 \langle f(R) \rangle_{\nu\nu} + 2 \sum_{\nu \neq \nu'} c_{\nu'}^* c_{\nu} \cos(\omega_{\nu'\nu} t) \langle f(R) \rangle_{\nu'\nu} \end{aligned} \quad (5)$$

with $f(R) = R, D(R)$ in our case, the vibrational frequency being $\omega_{\nu'\nu} = (E_{\nu'} - E_{\nu})/\hbar$, and

$$\langle f(R) \rangle_{\nu'\nu} = \int \varphi_{\nu'}^*(R) f(R) \varphi_{\nu}(R) dR, \quad (6)$$

Thus, $\langle f(R) \rangle_t$ oscillates around the average of the contributions of the populated vibrational levels, $\langle f(R) \rangle_{\nu\nu}$, weighted by $|c_{\nu}|^2$. The oscillatory behavior is governed by cross terms with frequencies $\omega_{\nu'\nu}$. In contrast to the constant rotational spacing of a rigid molecule, which determines also the rotational dynamics in a constant electric or laser field, the vibrational spacing typically decreases with increasing degree of excitation and the corresponding frequencies $\omega_{\nu'\nu}$ do not form a commensurate set. We also analyze the temporal evolution of the spatial delocalization of the wave packet using the variance

$$\sigma_R(t) = \sqrt{\langle R^2 \rangle_t - \langle R \rangle_t^2}. \quad (7)$$

III. VIBRATIONAL WAVE PACKET DYNAMICS

Our fit of a harmonic oscillator potential accounts properly for the repulsive barrier of the potential energy curve of CO, i. e., for $R < R_{min}$, see Fig. 1 (a). For its frequency we obtain 89 ± 16 THz. This ensures that the spreading of the wave packet remains within the CO potential energy curve.

In the coherent state Eq. (2), the two degrees of freedom of the parameter z , i. e., its real and imaginary parts z_R and z_I , play a similar role, and qualitatively similar results are obtained by keeping $|z|$ constant. By increasing $|z|$, the center of the initial coherent state is shifted towards larger values of R , which implies that higher energies within the vibrational spectrum are explored by the corresponding wave packet. In the next sections, we analyze the vibrational dynamics for the coherent states with $z = 1 + i$, $z = 5$ and $z = 4 + 4i$.

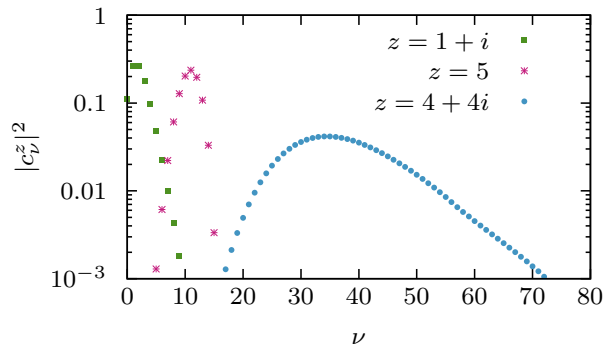


FIG. 2. Absolute value squared of the coefficients $|c_{\nu}^z|^2$ of the decomposition Eq. (3) in terms of the vibrational eigenstates of CO, for the coherent states with $z = 1 + i$ (green squares) $z = 5$ (pink stars) and $z = 4 + 4i$ (blue circles).

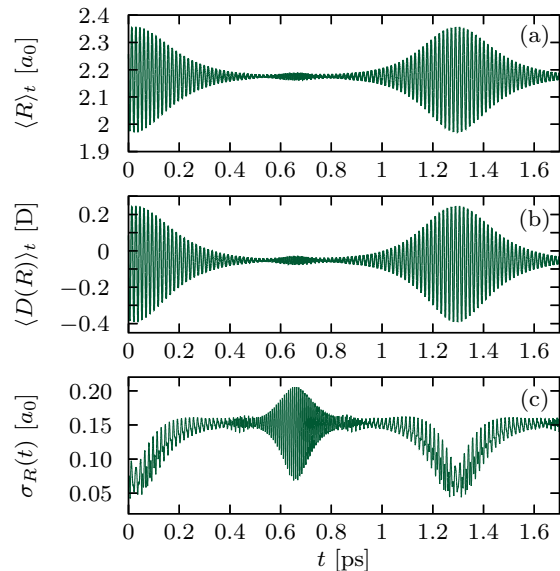


FIG. 3. Wave packet dynamics of the $z = 1 + i$ coherent state. Shown is the time evolution of the expectation values (a) $\langle R \rangle_t$ and (b) $\langle D(R) \rangle_t$, as well as (c) the variance $\sigma_R(t)$.

A. Wave packet dynamics for $z = 1 + i$

For the $z = 1 + i$ coherent state, only the lowest ten vibrational states of CO possess a weight larger than 10^{-3} in the expansion (4), with the vibrational eigenstates up to the third excited one having the dominant contributions as shown in Fig. 2. The energy of this wave packet is relatively small, -0.386 Hartree, and lies between the $\nu = 3$ and $\nu = 4$ eigenstates of CO. Hence, its vibrational dynamics is confined to the lower part of the CO potential energy curve as illustrated in Fig. 1 (a). The time evolutions of $\langle R \rangle_t$, $\langle D(R) \rangle_t$, and $\sigma_R(t)$ are presented in Fig. 3. $\langle R \rangle_t$ and $\langle D(R) \rangle_t$ show an oscillatory behavior around the mean values $2.18 a_0$ and -0.05 D, respec-

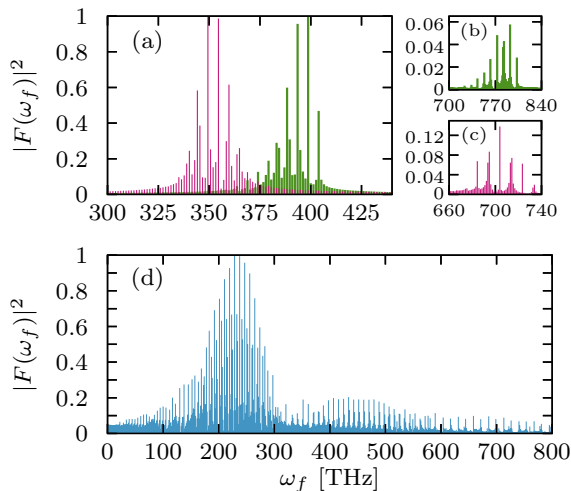


FIG. 4. Power spectrum obtained from the discrete Fourier transform of $\langle R \rangle_t$ for the coherent states (a) $z = 1 + i$ (thick green line) and $z = 5$ (thin pink line), and for (d) $z = 4 + 4i$ (thin blue line). Panels (b) and (c) show the power spectrum for a window of larger frequencies for $z = 1 + i$ and $z = 5$ wave packets, respectively. Note that $|F(\omega_f)|^2$ is normalized such that the maximum value equals one.

tively. Most important, the EDM of this wave packet oscillates rapidly between positive and negative values, the maximum value being $\langle D(R) \rangle_t = 0.24 D$ and the minimum one is $\langle D(R) \rangle_t = -0.39 D$.

The similar behavior of $\langle R \rangle_t$ and $\langle D(R) \rangle_t$ is due to the almost linear dependence of $D(R)$ on R in the relevant range of $V(R)$ covered by the vibrational dynamics (see Fig. 1 (b)). They both show rapid oscillations, with a frequency of approximately 393.5 THz, and a period of approximately 0.016 ps. The amplitudes are modulated by a slower frequency corresponding to 4.9 THz, which is responsible for the long time revival at $t \approx 1.28$ ps. The discrete Fourier transform of $\langle R \rangle_t$ is presented in Figs. 4 (a) and (b). The frequencies due to nearest neighbor vibrational states $\omega_{\nu+1,\nu}$ are dominant and can clearly be observed in Fig. 4 (a). Indeed, the large and small frequencies dominating the vibrational dynamics are approximately given by $(\omega_{1,2} + \omega_{2,3})/2$ and $\omega_{2,3} - \omega_{1,2}$, with $\omega_{1,2} = 398.7$ THz and $\omega_{2,3} = 393.8$ THz. The frequencies due to the next nearest vibrational neighbors, $\omega_{\nu+2,\nu}$, are shown in panel (b) of Fig. 4, and their influence on the dynamics is rather small.

The spreading of the wave packet is illustrated in Fig. 3 (c) via the variance $\sigma_R(t)$ defined in Eq. (7). This is complemented by snapshots of the square of the absolute value of the wave packet for several time instants in Fig. 5. During the first oscillations, the wave packet maintains its Gaussian shape, but increases its FWHM and decreases its height while its center oscillates around the minimum of the potential well, as it is illustrated in panel (a) of Fig. 5 for the time instants $t = 0.0, 0.008$ and 0.013 ps. For $t = 0.068$ ps, the wave packet has become

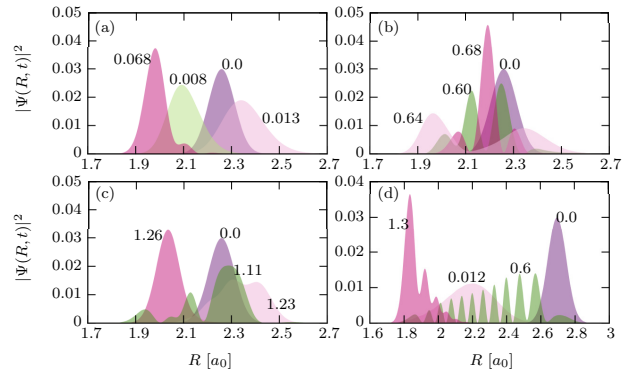


FIG. 5. The absolute value squared of the wave packet at different times, indicated in units of picoseconds in the panels, (a), (b) and (c) for the $z = 1 + i$ coherent state, and (d) for the $z = 5$ coherent state.

narrower, whereas its Gaussian shape starts to be more strongly distorted, manifesting itself in the existence of a pronounced asymmetry and a right-sided tail with a second maximum being visible.

Following the decay of the amplitude of the fast oscillations of $\langle R \rangle_t$ and $\langle D(R) \rangle_t$ (see Fig. 3 (a,b)) we observe for the time window $0.5 \text{ ps} \lesssim t \lesssim 0.9 \text{ ps}$ via the large values and large amplitude oscillations of the variance in Fig. 3 (c) a substantial spreading (and partial refocusing) of the wave packet. This is confirmed by the snapshots of the absolute square of the wave packet presented in Fig. 5 (b). It is now spread over the entire region between the classical turning points of the potential, and exhibits several maxima, due to the contribution of several vibrational eigenstates. With further increasing propagation time, the mean value of $\sigma_R(t)$ first remains approximately constant but then starts to decrease for $t \gtrsim 1.1$ ps thereby approaching the first revival. In this region, the wave packet is initially spread over large parts of the potential but becomes more localized again during the revival as illustrated in Fig. 5 (c) for $t = 1.26$ ps.

B. Wave packet evolution for $z = 5$

For the $z = 5$ coherent state, higher excited eigenstates contribute substantially to its time evolution (4), and the dominant vibrational excitations are those for $10 \leq \nu \leq 13$, see Fig. 2. The wave packet possesses a larger energy -0.319 Hartree, i.e., it lies energetically between the $\nu = 9$ and $\nu = 10$ vibrational eigenstates. Thus, a larger range within the potential energy curve is accessible for the vibrational dynamics as illustrated in Fig. 1 (a). The dynamics of the observables $\langle R \rangle_t, \langle D(R) \rangle_t$ in Fig. 6 shows a qualitatively similar but quantitatively different behavior as for the $z = 1 + i$ coherent state in Fig. 3. The expectation values $\langle R \rangle_t$ and $\langle D(R) \rangle_t$ rapidly oscillate in time with a smaller frequency of 351 THz, and these oscillations possess larger ampli-

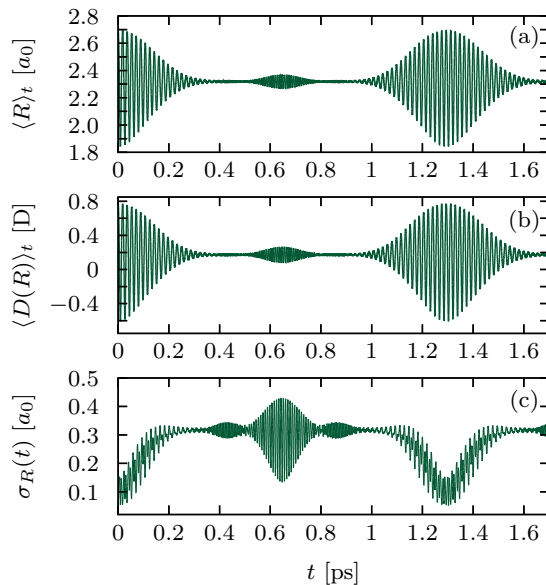


FIG. 6. Wave packet dynamics of the $z = 5$ coherent state. Time evolution of the expectation values (a) $\langle R \rangle_t$ and (b) $\langle D(R) \rangle_t$, as well as (c) the variance $\sigma_R(t)$.

tudes due to the contribution of higher excited vibrational states. These fast oscillations are again modulated by a smaller frequency of 4.9 THz, contributing to the observed decay and revival. The averages of $\langle R \rangle_t$ and $\langle D(R) \rangle_t$ are shifted to larger values $2.31 a_0$ and $0.17 D$, respectively. As for the $z = 1 + i$ coherent state, $\langle D(R) \rangle_t$ shows also for $z = 5$ oscillations corresponding to an alternating sign of the dipole moment with a maximum value of $0.77 D$ and a minimum value of $-0.60 D$.

The frequencies obtained from the discrete Fourier transform of $\langle R \rangle_t$ are presented in Figs. 4 (a) and (c). The energy gap between neighboring vibrational levels is reduced as we move energetically up in the CO vibrational spectrum. This explains that the dominant frequencies in $\langle R \rangle_t$ are smaller compared to those of the $z = 1 + i$ coherent state, see the pink versus green histograms in Fig. 4 (a). The rapid oscillations of $\langle R \rangle_t$ can be explained in terms of $(\omega_{11,12} + \omega_{12,13})/2$ and the frequency modulating their amplitude is $\omega_{12,13} - \omega_{11,12}$, with $\omega_{11,12} = 354.4$ THz and $\omega_{12,13} = 349.6$ THz.

The variance in Fig. 6 (c) indicates a larger spreading of the wave packet, which is also illustrated by the snapshots at several times in Fig. 5 (d). The spatial width of the wave packet is larger, and the contribution of higher excitations is reflected in the presence of more maxima as a function of the internuclear distance R .

C. Wave packet dynamics for $z = 4 + 4i$.

By further increasing $|z|$, the decomposition (3) of the coherent state involves more eigenstates with a signifi-

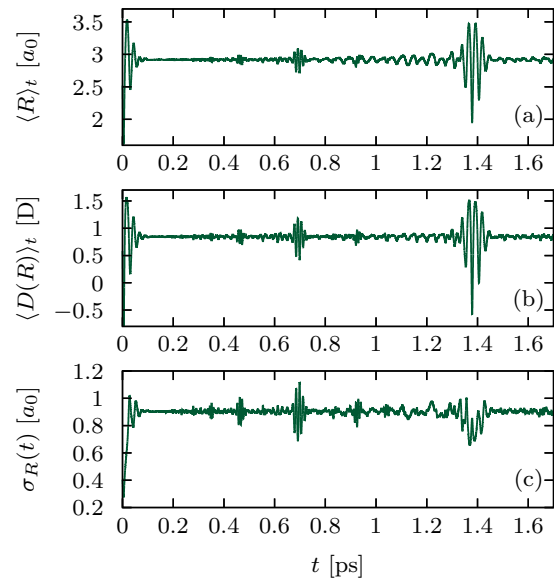


FIG. 7. Wave packet dynamics of the $z = 4 + 4i$ coherent state. Time evolution of the expectation values (a) $\langle R \rangle_t$ and (b) $\langle D(R) \rangle_t$, as well as (c) the variance $\sigma_R(t)$.

cant weight. This implies that more frequencies participate in the resulting dynamics and, as a consequence, the characteristic oscillations of the expectation values observed in the previous cases might disappear. For instance, in the expansion (3) of the $z = 4 + 4i$ wave packet the eigenstates within the vibrational range $28 \leq \nu \leq 55$ ($18 \leq \nu \leq 72$) possess weights larger than 10^{-2} (10^{-3}), see Fig. 2. Energetically, this coherent state with an energy -0.121 Hartree lies between the $\nu = 37$ and $\nu = 38$ vibrational eigenstates, and has a larger internuclear region to explore as shown in Fig. 1 (a).

This large number of vibrational states with similar weights significantly impacts the dynamics as illustrated by the time evolutions of $\langle R \rangle_t$ and $\langle D(R) \rangle_t$ in Fig. 7 (a) and (b), respectively. $\langle R \rangle_t$ and $\langle D(R) \rangle_t$ do not show regular oscillations due to the many frequencies with a similar contribution. A rapid decay within the first few oscillations is observed followed by an irregular behavior with occasionally occurring partial revivals. The corresponding power spectrum of $\langle R \rangle_t$ is presented in Fig. 4 (d) demonstrating the broad bands of contributing frequencies. Severe differences occur in comparison to the power spectrum of the wave packets belonging to $z = 1 + i$ and $z = 5$ presented in panel (a) can be observed. For example, and among others, there are now six frequencies with a contribution larger than 0.8.

A few more specific remarks are in order. Initially $\langle R \rangle_t$ and $\langle D(R) \rangle_t$ show rapid oscillations, in which $\langle D(R) \rangle_t$ is, during a certain interval of the oscillatory motion, negative for approximately only 6 fs. After these few fast oscillations at short times, the dipole moment remains approximately constant and positive with small ampli-

tude deviations. As expected, due to the participation of higher excited vibrational eigenstates in the wave packet dynamics, the mean values of $\langle R \rangle_t$ and $\langle D(R) \rangle_t$ are larger as compared to the previously analyzed coherent state dynamics. The observed half and full revivals remain as characteristic features of the dynamics, and between them several irregular oscillatory bursts of motion are encountered. During the full revival, $\langle D(R) \rangle_t$ is negative for the very short period of 5 fs only. These short time intervals where $\langle D(R) \rangle_t$ changes sign and becomes negative also appear for coherent states with even larger values of $|z|$. The variance $\sigma_R(t)$, shown in Fig. 7 (c), also presents a distinctly different time evolution compared to the previous cases. Its large value indicates that the wave packet is delocalized and spreads over large parts of the potential energy curve in the course of the dynamics.

IV. CONCLUSIONS

Motivated by the recently found Rydberg atom-ion molecules with a molecular bond that shows a flipping dipole [26, 27] we explore in this work the vibrational dynamics of a wave packet within the electronic ground state of the CO molecule. Our specific choice is well-grounded in the fact that CO possesses an electronic dipole moment function that has (approximately) a zero crossing at the equilibrium internuclear distance, with negative/positive dipole moments for smaller/larger internuclear separations. We have constructed coherent wave packets for different parameter values as initial states for our study of the dynamical evolution. Several relevant observables such as the mean internuclear separation $\langle R \rangle_t$, the dipole moment $\langle D(R) \rangle_t$ as well as the variance $\sigma_R(t)$ of the wave packet have been analyzed.

For low and moderate values of the coherent state parameter $|z|$, the coherent state lies in the lower part of the vibrational spectrum of CO. It can be expressed as a superposition of a relatively small number of vibrational states, and the time evolutions of $\langle R \rangle_t$ and $\langle D(R) \rangle_t$ are dominated by two frequencies. Consequently the wave packet performs spatial oscillations in time close to the potential minimum where $D(R)$ changes its sign. Therefore, we encounter a flipping dipole moment taking on

both positive and negative values during the corresponding phases of the evolution. Such a behavior cannot be realized on basis of a pure rotational dynamics including electric or non-resonant laser fields due to the smaller energy scales involved. Apart from fast oscillations we encounter a slow decay and subsequent (fractional) revivals of the wave packet which is accompanied by a similar characteristic behavior of the dipole moment.

By increasing $|z|$, the wave packet possesses a larger energy, explores a larger internuclear range, and higher and more vibrational excitations control the dynamics. The many contributing non-commensurable vibrational frequencies lead to a rapid decay of the fast oscillations of $\langle R \rangle_t$ and $\langle D(R) \rangle_t$, but still the half and full revivals appear as characteristic features of their time evolution, although taking place at irregular time intervals. Interestingly, $\langle D(R) \rangle_t$, which is now positive, reaches negative values only during the case of a complete revival.

A few comments concerning the experimental implementation of our setup are in order. The preparation of the coherent state of the CO vibrational dynamics could be accomplished by ensuring the proper populations of the (few most relevant) excited states, ideally using an optimally designed light pulse providing the proper phase relationship [33–35]. Concerning the observation of the coherent state dynamics and in particular the flipping dipole dynamics a pump probe spectroscopy might pave the way as it is used frequently in the literature [36].

Taking the present work as a starting-point for future investigations, one could envisage to explore other diatomic systems with a similar or complementary structure of the dipole moment function. It is an open route of exploration to construct corresponding wave packets for polyatomic systems with several vibrational degrees of freedom that might show an even more intriguing dynamics of the corresponding dipole or higher moments.

ACKNOWLEDGMENTS

C.B. and R.G.F. gratefully acknowledge financial support by the Spanish projects PID2020-113390GB-I00 (MICIN), and PY20-00082 (Junta de Andalucía), and the Andalusian research group FQM-207.

-
- [1] T. Helgaker, P. Jørgensen and J. Olsen, *Molecular Electronic-Structure Theory*, Wiley (2013).
 - [2] A. Szabo and N.S. Ostlund, *Modern Quantum Chemistry: Introduction to Advanced Electronic Structure Theory*, Dover Books on Chemistry (1996).
 - [3] R.J. Bartlett and M. Musiał, *Rev. Mod. Phys.* **79**, 291 (2007).
 - [4] N. Mardirossian and M. Head-Gordon, *Mol. Phys.* **115**, 2315 (2017).
 - [5] C.J. Pethick and H. Smith, *Bose-Einstein Condensation in Dilute Gases*, Cambridge University Press (2011).
 - [6] R. Grimm, M. Weidemüller and Y.B. Ovchinnikov, *Adv. At. Mol. Opt. Phys.* **42**, 95 (2000).
 - [7] C. Chin, R. Grimm, P. Julienne and E. Tiesinga, *Rev. Mod. Phys.* **82**, 1225 (2010).
 - [8] M. Lewenstein, A. Sanpera, V. Ahufinger, B. Damski, A. Sen and U. Sen, *Adv. Phys.* **56**, 243 (2007).
 - [9] M. Lewenstein, A. Sanpera and V. Ahufinger, *Ultracold Atoms in Optical Lattices Simulating Quantum Many-Body Systems*, Oxford University Press (2012).
 - [10] C.H. Greene, P. Giannakeas and J. Perez-Rios, *Rev. Mod. Phys.* **89**, 0035006 (2017).

- [11] T. Gallagher, Rydberg Atoms, Cambridge University Press (1994).
- [12] C. Fey, F. Hummel and P. Schmelcher, Mol. Phys. **118**, e1679401 (2020).
- [13] C.H. Greene, A.S. Dickinson, and H.R. Sadeghpour, Phys. Rev. Lett. **85**, 2458 (2020).
- [14] V. Bendkowsky *et al*, Nature **458**, 1005 (2009).
- [15] V. Bendkowsky *et al*, Phys. Rev. Lett. **105**, 163201 (2010).
- [16] W. Li *et al*, Science **334**, 1110 (2011).
- [17] J. Tallant *et al*, Phys. Rev. Lett. **109**, 173202 (2012).
- [18] J.B. Balewski *et al*, Nature **502**, 664 (2013).
- [19] A. Gaj *et al*, Nat. Commun. **5**, 4546 (2014).
- [20] B.J. DeSalvo *et al*, Phys. Rev. A **92**, 031403(R) (2015).
- [21] F. Camargo *et al*, Phys. Rev. Lett. **120**, 083401 (2018).
- [22] F. Engel *et al*, Phys. Rev. Lett. **123**, 073003 (2019).
- [23] F. Hummel *et al*, New J. Phys. **22**, 063060 (2020).
- [24] A. Duspayev *et al*, Phys. Rev. Res. **3**, 023114 (2021).
- [25] M. Deiß, S. Haze and J. Hecker-Denschlag, Atoms **9**, 34 (2021).
- [26] N. Zuber *et al*, Nature **605**, 453 (2022).
- [27] Y.-Q. Zou *et al*, Phys. Rev. Lett. **130**, 023002 (2023).
- [28] R. González-Férez and P. Schmelcher, Phys. Rev. A **69**, 023402 (2004).
- [29] A. Le Floch, Mol. Phys. **72**, 149 (1991)
- [30] A. Galindo and P. Pascual, Quantum Mechanics I, Springer, Second Edition (1989).
- [31] M.O. Scully and M. Zubairy, Quantum Optics, Cambridge University Press (1997).
- [32] C. Chackerian, private communication; C. Chackerian, J. Chem. Phys. **65**, 4228 (1976).
- [33] A. P. Peirce, M. A Dahleh, and H. Rabitz. Phys. Rev. A **37**, 4950 (1988).
- [34] J. Werschnik and E.K.U. Gross, J. Phys. B: At. Mol. Opt. Phys. **40** R175 (2007).
- [35] C. Brif, R. Chakrabarti, and H. Rabitz. N. J. Phys. **12** 075008 (2010).
- [36] W.W. Parson and C. Burda, Modern Optical Spectroscopy: From Fundamentals to Applications in Chemistry, Biochemistry and Biophysics, 3rd edition, Springer (2023).